ChemPubSoc Europe

DOI: 10.1002/cctc.201402602

Eco-Friendly Catalytic Systems Based on Carbon-Supported Magnesium Oxide Materials for the Friedländer Condensation

Marina Godino-Ojer,[a] Antonio J. López-Peinado,[a] Rosa M. Martín-Aranda,[a] Jacek Przepiórski,[b] Elena Pérez-Mayoral,*[a] and Elena Soriano*[c]

Carbon-supported MgO materials are excellent and sustainable catalysts for the synthesis of N-containing heterocyclic compounds by the Friedländer condensation under mild, solvent-free conditions. The results reported herein indicate that MgO is the most active catalytic species that accelerates the reaction compared with the catalytic behavior observed for the carbon material Norit RX3. On the basis of DFT calculations, a reaction mechanism that involves dual activation of the reacting structures by the catalyst is proposed.

Introduction

The Friedländer condensation, which proceeds through double condensation between 2-aminoaryl carbonyl components with other carbonyl compounds with active methylene groups, is one of the most cited and useful reactions in organic synthesis.[1] It is the method of choice for the synthesis of a large variety of N-containing heterocyclic compounds such as quinolines,[2] naphthyridines,[3] and acridones.[4] These N-containing heterocyclic systems are present in many naturally occurring products and synthetic drugs associated with several versatile pharmacological activities, which make them interesting target compounds for use in medicine and other fields. The structures of some biologically active heterocyclic rings are shown in Figure 1; compound **1** derived from 2-aminobenzaldehyde is a known histone acetyltransferase inhibitor,[5] whereas naphthyridine **2**[6] and acridone **3**[4] exhibit antimicrobial and anticancer activity, respectively.

Several heterogeneous catalytic systems have been reported for the synthesis of this type of N-heterocyclic compounds by the Friedländer reaction such as Al_2O_3,[7] acids supported on silica gel,[8] silica propylsulfonic acid,[9] and AlKIT-5.[10] Notably, most of these have acidic properties, whereas the investigation of basic materials is almost neglected. In addition, this condensation has been explored preferentially starting from the corresponding 2-aminoaryl ketones in an acidic medium.

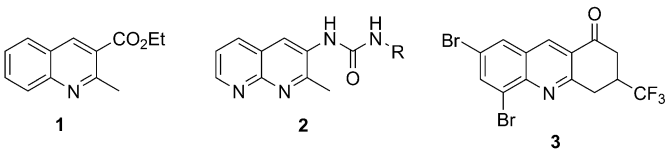

Figure 1. Biologically active N-containing heterocyclic compounds.

Our research group works on the development of new, environmentally friendly, and efficient catalytic materials for applications in green processes, and the Friedländer condensation occupies an important place in our investigations. In this sense, several catalysts have been reported that differ in composition, structure, and porosity, which include zeolites,[11] acidic, basic, and bifunctional mesoporous silicas,[12] metal–organic frameworks, particularly copper-1,3,5-benzenetricarboxylate,[13] and carbon materials.[14] Our studies often concern interesting mechanistic revelations that result from the combination of experimental results with computational methods.

Our latest results indicated that the condensation of 2-aminoaryl aldehydes **4**, which are substrates that are barely investigated in heterogeneous catalysis, proceeds regioselectively. Thus, in the presence of amino-functionalized T/MCF (T = Nb or Al, MCF = mesostructured cellular foams), which probably acts as a bifunctional catalytic system (Scheme 1),[12c–d] the corresponding quinolones **5b** and **e** are formed.

As a continuation of our studies, we report herein the first basic hybrid carbon materials as efficient heterogeneous catalytic systems for the synthesis of quinolines, naphthyridines, and acridones by the Friedländer condensation using 2-aminoaryl aldehydes and different carbonyl components as substrates. Additionally, we have investigated the reaction mechanism computationally and focused mainly on the catalytic steps that take place during the synthesis of **5**.

[a] M. Godino-Ojer, Prof. A. J. López-Peinado, Prof. R. M. Martín-Aranda, Dr. E. Pérez-Mayoral
Departamento de Química Inorgánica y Química Técnica
Universidad Nacional de Educación a Distancia, UNED
Paseo Senda del Rey 9, 28040 Madrid (Spain)
E-mail: eperez@ccia.uned.es

[b] Dr. J. Przepiórski
Institute of Chemical and Environmental Engineering
West Pomeranian University of Technology
Pulaskiego 10, 70-322 Szczecin (Poland)

[c] Dr. E. Soriano
Instituto de Química Orgánica General, CSIC
C/Juan de la Cierva 3, 28006 Madrid (Spain)

Supporting information for this article is available on the WWW under http://dx.doi.org/10.1002/cctc.201402602.

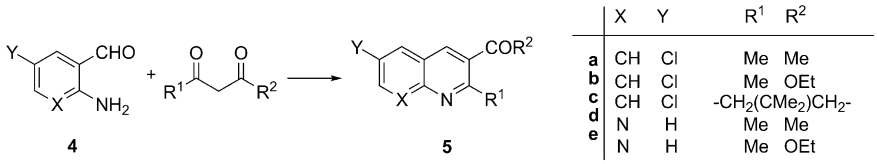

Scheme 1. Friedländer condensation of 2-aminobenzaldehydes **4**.

Results and Discussion

Catalysts were synthesized by using the synthetic methodology reported previously by Przepiorski and co-workers.[15] Thus, carbon-supported MgO materials were prepared by the calcination (923 K) of homogeneous mixtures of poly(ethylene terephthalate) (PET) and magnesite (MAG), which served as the carbon source and MgO precursor, respectively.

The textural parameters of the commercial Norit RX3 and the hybrid carbon-MgO materials under study together with the MgO loadings are shown in Table 1. Compared to the hybrid materials, the MgO-free activated carbon has a predominantly microporous character. In addition, it shows a considerably higher specific surface area than the other materials, which concerns both micropores and mesopores. However, the combined materials are rich in basic MgO and reveal a bimodal, microporous–mesoporous character. In general, the pore structure parameters calculated for these porous systems tend to decrease with the MgO loading, and the relative contribution of microporosity to the total surface in these materials shows the reverse order.

Table 1. Characterization of the investigated basic carbon materials.

Catalyst[a]	S_{BET} [m^2g^{-1}]	S_{total}[b] [m^2g^{-1}]	S_{ext}[b] [m^2g^{-1}]	S_{micro}[b] [m^2g^{-1}]	MgO loading [wt%]	Mean MgO crystallite size [nm]	pH_{PZC}
PET/MAG 70:30	370	480	160	320	53	13.0	10.16
PET/MAG 50:50	240	279	136	143	65	23.5	10.21
PET/MAG 30:70	206	223	115	68	78	24.6	10.23
Norit RX3	1306	1468	191	1277	–	–	7.4[c]

[a] Poly(ethylene terephthalate) (PET) and Magnesite (MAG). The values that follow correspond to the PET/MAG ratios. [b] *S* is the surface area calculated by using the α-method. See Ref. [15]. [c] See Ref. [14].

As reported previously,[16] the mean size of MgO crystallites included in the hybrid materials tends to decrease with PET/MAG ratio. The results of XRD examinations reported elsewhere[15] confirmed a small amount of impurities, mainly silica, which originates from the MAG.

We studied the acid–base properties of the hybrid carbon-MgO materials by determining the pH_{PZC} values (pH at the point of zero charge) following the experimental protocol reported by Valente Nabais and Carrot.[17] As a result of the presence of MgO, the hybrid materials under study exhibited basic properties with a pH_{PZC} value in the range of 10.16–10.21, considerably higher than that of the carbon Norit RX3 as expected (Table 1).

The catalytic performance of porous carbon/MgO hybrids with different MgO contents was first investigated in the Friedländer condensation of 2-amino-5-chlorobenzaldehyde (**4a**) and acetylacetone ($R^1 = R^2 = Me$) under solvent-free conditions at room temperature (293 K). Thus, the condensation reaction catalyzed by PET/MAG 30:70 and PET/MAG 50:50 led to the corresponding quinolone **5a** in almost 90% yield after 4 h (Scheme 1; Table 2, entries 2–3). The conversion to **5a** depends on the PET/MAG ratio, and PET/MAG 70:30 is the least efficient catalyst (Figure 2). Besides the observed differences in the textural parameters, the carbon-supported MgO samples under study showed different sizes of MgO crystallites as a function of their MgO loadings (Table 1). In this sense, the observed activity of the catalysts does not only correlate with the MgO loading but also with the increased number of active catalytic sites over the MgO crystal surface. Notably, the carbons that include large MgO crystallites (PET/MAG 50:50 and PET/MAG 30:70) and the highest MgO loadings afforded **5a** with increased yields, whereas PET/MAG 70:30, in which the size of the MgO crystals is considerably smaller, led to decreased yields to **5a**. Although the mean crystallite sizes of MgO of the hybrid materials PET/MAG 50:50 and PET/MAG 30:70 were comparable, but slightly higher for PET/MAG 30:70, the improved yield of **5a** in the process catalyzed by PET/MAG 30:70, at the beginning of the reaction, is probably because of the high available surface of MgO crystals. However, in both cases, compound **5a** was obtained with similar conversions after prolonged reaction times; this effect could be because of the diffusion of reagents and product through the channels.

Table 2. Friedländer reaction between 2-aminoaryl aldehydes (**4**) and 1,3-dicarbonyl compounds.

Entry	Catalyst	Product	Time [min]	Yield to **5** [%]
1	PET/MAG 70:30	**5a**	240	79
2	PET/MAG 50:50	**5a**	240	88
3	PET/MAG 30:70	**5a**	240	89
4	PET/MAG 30:70	**5a**	240	75[a]
5	PET/MAG 30:70	**5a**	240	76[b]
6	Norit RX3[c]	**5a**	240	39
7	PET/MAG 30:70	**5b**	60 (15)[d]	71 (99)[d]
8	PET/MAG 30:70	**5c**	15	97[e]
9	PET/MAG 30:70	**5d**	60	98[d]

[a] Catalyst amount: 50 mg. [b] Catalyst amount: 12 mg. [c] See Ref. [11]. [d] Reaction temperature 323 K. [e] Reaction temperature 347 K.

We also compared the catalytic performance of MgO-containing carbons with that exhibited by a commercial carbon, Norit RX3.[14] The yield of **5a** versus time for the reaction catalyzed by Norit RX3, a microporous activated carbon with

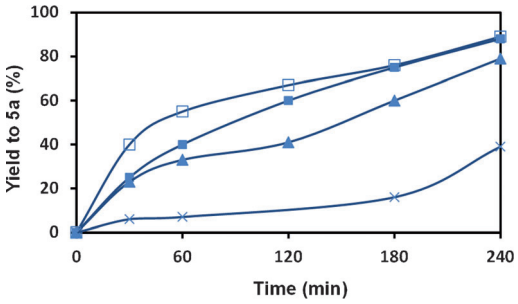

Figure 2. Friedländer reaction between **4a** and acetylacetone ($R^1 = R^2 = Me$) under solvent-free conditions at room temperature catalyzed by PET/MAG 30:70 (□), PET/MAG 50:50 (■), PET/MAG 70:30 (▲), and Norit RX3 (×).

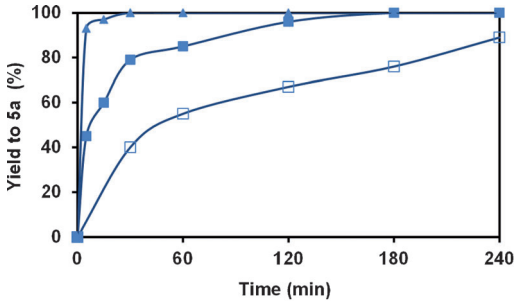

Figure 3. Friedländer reaction between **4a** and acetylacetone ($R^1 = R^2 = Me$) under solvent-free conditions catalyzed by PET/MAG 30:70 at 293 (□), 303 (■), and 323 K (▲).

a high surface area (S_{BET}; 1306 m^2g^{-1}) and a pH_{PZC} around 7.4, to give **5a** with an expected low yield is shown in Figure 2, and the results are also summarized in Table 2, entry 6. This circumstance could be attributed to the lower basicity of this carbon but also to a change in the operative pathway and hence in the reaction mechanism. Importantly, the conversions to **5a** on using amino-functionalized MCF materials[12c–d] was almost negligible after prolonged reaction times despite the higher temperatures (323 K).

These results suggest that the MgO content is a critical factor in the catalytic behavior of the hybrid carbon/MgO materials under study. We observed an increased yield to **5a** if the total surface area and the microporosity of the materials are notably decreased; these features were probably caused by the presence of increased amounts of MgO. The presence of MgO in these materials accelerates the reaction considerably and, hence, could be considered as the catalytically active species that plays a crucial role in the efficient formation of **5a**.

With these results in mind, further experiments were performed by using the carbon material with the highest MgO loading, PET/MAG 30:70, under the same experimental conditions.

In addition, we performed a study of the effect of the reaction temperature in the condensation between **4a** and acetylacetone. The yield to **5a** improved considerably at higher temperatures as expected (Figure 3). Thus, it was possible to obtain **5a** in quantitative yield after 2.25 h and 15 min at 303 and 323 K, respectively.

We also examined the influence of the catalyst amount for PET/MAG 30:70 in the reaction of **4a** and acetylacetone (Table 2; entries 3–5). The condensation proceeds even in the presence of a small amount of PET/MAG 30:70 (12 mg) to afford **5a** in 75% yield after 4 h. However, if we used more catalyst (50 mg), the yield to **5a** was maintained (Figure 4). The experimental data then indicate that there is an optimum concentration of the catalyst (25 mg) to lead to **5a** in the highest yield after 4 h. This confirms an additional advantage of using MgO-containing porous carbons in the efficient synthesis of N-containing heterocycles that is minimum waste production.

We then demonstrated that the basic carbons under study, particularly that with the highest MgO loading, PET/MAG 30:70, are efficient catalysts for the Friedländer condensation

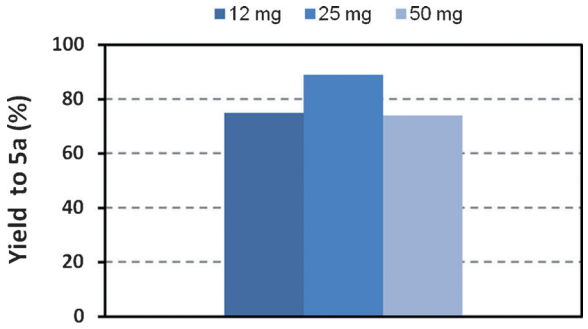

Figure 4. Influence of the catalyst amount on the Friedländer reaction between **4a** and acetylacetone ($R^1 = R^2 = Me$) under solvent-free conditions at room temperature catalyzed by PET/MAG 30:70 after 4 h of reaction time.

under mild reaction conditions to afford **5a** in excellent yields even if a small amount of the solid is used.

To explore the scope of the methodology reported herein, we studied the Friedländer reaction using different 2-aminoaryl aldehydes and other carbonyl components with enolizable H atoms. In this sense, the corresponding naphthyridine **5d** was also prepared, in the presence of PET/MAG 30:70 at room temperature in 60% yield after 4 h. The yield to **5d** increased if the temperature was increased to 323 K to obtain almost pure **5d** in only 1 h (Figure 5; Table 2, entry 9).

However, the condensation between **4a** and an asymmetric carbonyl compound, the ethyl acetoacetate ($R^1 = Me$; $R^2 = OEt$), allowed us to investigate the regioselectivity of the reaction (Scheme 1). Compound **1** (related to **5b**) has been reported as a building block for the synthesis of *lavendamycin* analogues.[18] Thus, the reaction catalyzed by PET/MAG 30:70 yielded quinolone **5b** exclusively in 71% (1 h) and in a quantitative yield (15 min) at room temperature and at 323 K, respectively (Table 2, entry 7).

Finally, acridone **5c** (related to biologically active **3**) was synthesized by the reaction of **4a** and dimedone (R^1–$R^2 = CH_2C(Me)_2CH_2$). The reaction was performed in the presence of PET/MAG 30:70 at 347 K, as both starting materials are solid compounds, to lead to **5c** in 97% yield after only 15 min (Table 2, entry 8).

The catalytic behavior of MgO-containing carbons in the condensation of **4a** with ethyl acetoacetate was quite similar

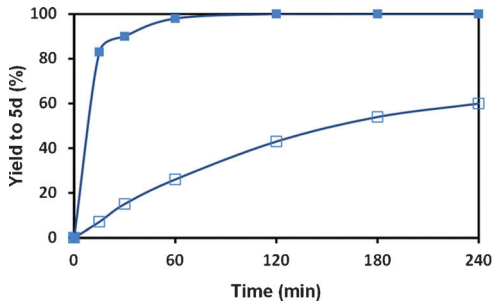

Figure 5. Friedländer reaction between **4d** and acetylacetone catalyzed by PET/MAG 30:70 under solvent-free conditions at room temperature (□) and 323 K (■).

to that observed for [3-(2-aminoethylamino)propyl]trimethoxysilane/MCF, the most efficient amino-grafted mesoporous silica reported previously for this transformation.[12c] In this sense, the basic carbons reported herein are cheap and environmentally friendly alternative catalysts with remarkable thermal stability.

The results presented above have been rationalized by using computational methods. Although the carbon-based support has a slight influence in the condensation reaction, the investigation of the reaction mechanism was performed using only MgO as the predominant active catalytic species. The lower activity found for Norit RX3 could be rationalized by the π–π stacking interactions between the aromatic rings of the carbon material and **4a**, which probably modify the electrophilic and nucleophilic character of the −CHO and $-NH_2$ substituents. This approach has been proposed as an alternative to the classical acid catalysis described by Versées et al.[19] It has been reported that π–π stacking interactions can alter the acid–base properties of pyridine[20] and phenol.[21]

The oxides of alkaline earth metals such as MgO, BaO, and CaO are known for their basic properties, related mainly to the strong Lewis basicity of the surface O_2^- anions.[22] It is believed that several reactions of catalytic interest comprise primarily the rupture of a heterolytic bond in which the basic character of an O_2^- anion combines with the acid character of a Mg^{2+} cation.[23] Nevertheless, the acidic character of Mg cations predominates in the case of molecular adsorption,[24] in which the molecule resides on the cationic site. These properties of MgO make it a good catalyst for several catalytic reactions, such as the dehydrogenation of alcohols,[25] aldol condensation,[26] hydrogenation of olefins,[22] and transesterification of alkyl esters to produce biodiesel.[27]

Several molecules (alcohols,[28] H_2,[29] CH_4,[30] H_2O,[31] NO_2,[32] H_2S,[33] HCl,[34] CO,[35] CO_2 and SO_2,[36] O_2^-, and CO^-[37]) have been considered regarding the adsorption equilibrium geometry and the possibility of an eventual molecular dissociation. Thus, the first step of the most basic reaction is a deprotonation process, which leads to a dissociated structure (Scheme 2).

Initially, we studied the adsorption of the reactants on the oxide surface. The enolic dicarbonyl can be adsorbed or it can be dissociated chemically into two fragments on the surface of MgO crystals. However, all our efforts to locate the transition structure for the first adsorption mode were unsuccessful. In contrast, it can be envisaged that the dicarbonyl compound, which bears three O atoms, could be adsorbed dissociatively by three different modes, namely, through 1) one of the carbonyl groups (**R0a** and **R0b**) or 2) the carboxylic O atom (**R0c**). The calculations for all three studied scenarios suggest that the first adsorption mode drives the reaction to the most stable reactant complex with adsorption free energies of −17.2 and −15.9 kcal mol^{-1}, respectively, whereas the interaction through the ester O atom leads to a metastable complex that is 2.5 kcal mol^{-1} less stable than the isolated reactants. That is, dissociative chemisorption to form **R0a** and **R0b** is energetically favorable. These results and the absence of transition structures have been confirmed by exhaustive relaxed scan calculations of the potential energy surface (PES).

Subsequently, the second reactant species, the aldehyde, binds to the complex (Figure 6) through the Lewis acid properties of the catalyst through the carbonyl O atom lone pair interaction with a coadsorption energy of 37.5–43.0 kcal mol^{-1} (**R1a–c**). The carbonyl bond length of the aldehyde increases from 1.219 to 1.246–1.249 Å.

According to the three possibilities, the nucleophilic addition to the aldehyde can proceed through three transition structures (**TS1a–c**), the evolution of which lead to the intermediates **I1a–c**, respectively. The transition structure **TS1a** shows the shortest distance for the formation of the C–C bond (1.984 Å), whereas the largest value is found for **TS1c** (2.123 Å). The C–C bond is fully formed in **I1a–c** (1.616–1.625 Å). During this step, the adsorbed proton remains bound strongly to the catalyst (O–H bond 0.980–1.007 Å) and forms

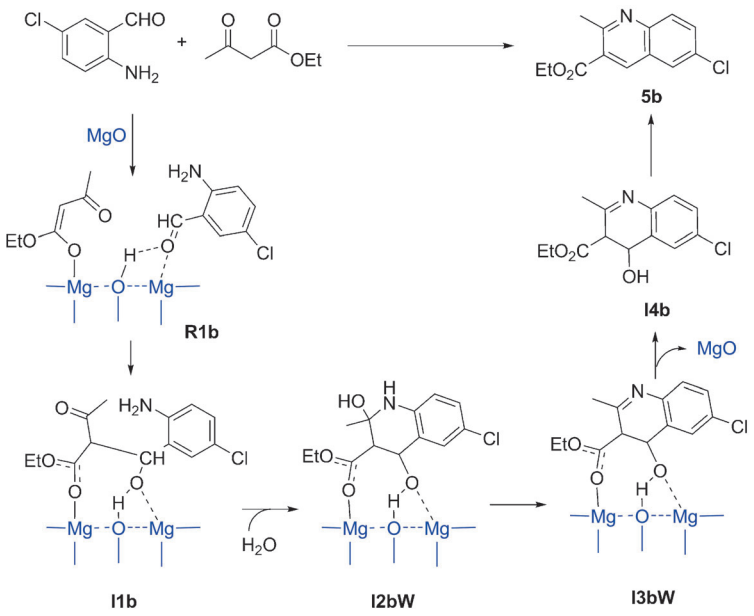

Scheme 2. Reaction mechanism for the Friedländer reaction between **4a** and ethyl acetoacetate (R^1 = Me; R^2 = OEt) catalyzed by carbon-supported MgO materials.

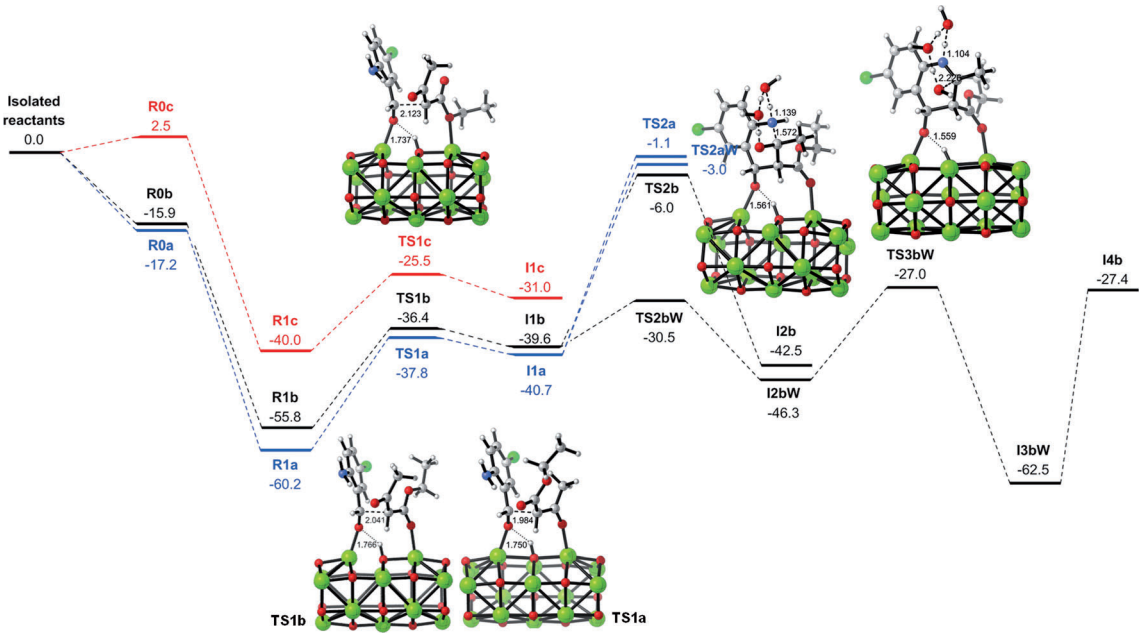

Figure 6. Free-energy profile [kcal mol^{-1}] for the condensation reaction between **4a** and ethyl acetoacetate catalyzed by MgO.

a strong H bond with the O atom of the carbonyl acceptor (1.737–1.766 Å for the transition structures **TS1**, 1.496–1.554 Å for the intermediates **I1**). Moreover, the O–Mg interaction through the carbonyl group is stronger than that through the ester O atom.

This step is endothermic and proceeds with moderate to high activation barriers. The formation of **I1a** is slightly favored kinetically over the formation of **I1b** but very favored over the formation of **I1c**, which suggests a lower catalytic effect through the O–Mg interaction through the ester O atom. Hence, we focus only on the former modes in the following discussion.

That the carbonyl O atom is bonded to Mg in the intermediates **I1a** and **b**, which has a critical impact on the regioselectivity as the following heterocyclization step should take place between the unbound carbonyl moiety and the amine group. First, we describe the heterocyclization of **I1b**. This step can proceed through **TS2b**, in which the N–C bond (1.657 Å) and O–H bond (1.388 Å) are partially formed. It drives the reaction to the heterocyclic intermediate **I2b** (N–C = 1.448, O–H = 0.966 Å). This process involves a very high activation barrier of 49.8 kcal mol^{-1} above **R1b**. Previous calculations on this step showed that traces of water can act as a bifunctional acid–base catalyst. Moreover, we found that, besides this strong kinetic effect, the presence of two molecules of water enhanced the regioselectivity for the formation of the quinoline framework.[12d] In line with these results, our current calculations reveal that the free-energy barrier for the cyclization catalyzed by two molecules of water (**TS2bW**) is reduced by 24.5 kcal mol^{-1} and shows an activation enthalpy, ΔH, of only 8.5 kcal mol^{-1}. The cyclized intermediate formed in this step, **I2bW**, then undergoes the elimination of water, which can be mediated by the two water molecules to alleviate the steric strain involved in the "dry" system. This elimination proceeds through **TS3bW**, which shows the advanced breaking of the C–OH bond (2.226 Å) and the initial leaving of the amine proton. This exothermic step (16.2 kcal mol^{-1}) proceeds with a moderate activation barrier and drives the reaction to the unsaturated bicycle **I3bW** and three molecules of water.

At this stage, **I3bW** should be desorbed from the active site to undergo a second dehydration step. Thus, the product desorption is a barrierless step, as the relaxed scan of the PES suggests, which generates the protonated adduct **I4b** by the breaking of the H–O(catalyst) bond. This step requires a free energy of 19.3 kcal mol^{-1}.[38] Once desorbed, the bicycle undergoes water-assisted dehydration to form the quinolone **5b**. This step takes place with a free-energy barrier of 18.5 kcal mol^{-1} via **TS4b**, which drives the reaction to the quinoline in a strongly exothermic step because of the formation of a highly stable aromatic product.

If we focus on the adsorption mode through the other carbonyl group, **R1a**, the nucleophilic attack of the amine in **I1a** takes place on the ester carbonyl C atom to form the bicyclic amide and ethanol. The transition structure **TS2a** (N–C = 1.616, C–OEt = 1.862 Å) involves a very high activation barrier (39.6 kcal mol^{-1}), which is 59.1 kcal mol^{-1} higher than that of **R1a**. Alternatively, the water catalysis reduces the Gibbs energy by only 1.9 kcal mol^{-1} (via **TS2aW**).[12d] Hence, these results indicate that this cyclization is strongly disfavored over the alternative route from a kinetic point of view and could account for the regioselectivity found at room temperature.

An inspection of the molecular orbitals provides further details. On the basis of Frontier molecular orbital theory, the smaller the energy difference between the LUMO level of the carbonyl acceptor and the HOMO level of amine in **I1**, the easier the electron transfer during nucleophilic attack and heterocyclization proceeds. For **I1a**, the HOMO–LUMO gap is calculated to be 4.12 eV, whereas for **I1b** it is decreased to

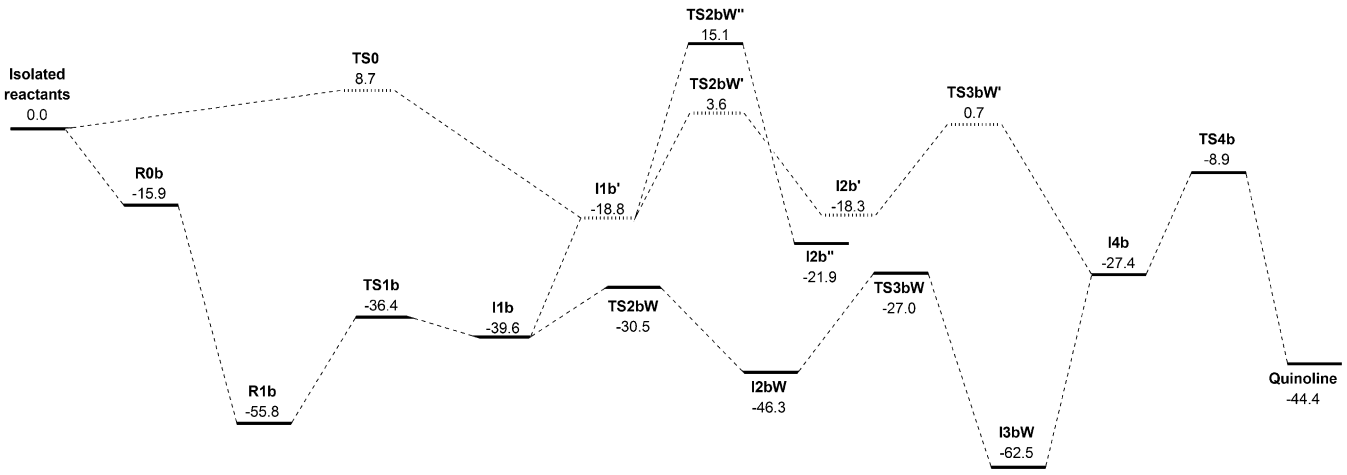

Figure 7. Comparison of the alternative reaction pathways computed for the condensation of **4** and ethyl acetoacetate to form **5 b** under MgO catalysis (solid line) and the uncatalyzed system (dashed line). The reaction path through the initial uncatalyzed Knoevenagel condensation is shown by a solid gray line.

3.53 eV. Furthermore, the LUMO coefficient at the carbonyl C atom is 0.232 for the former and 0.914 for the latter, so the orbital overlap should be more effective in **I1 b**.

We have also performed an equivalent simulation in the uncatalyzed gas-phase system for comparison. In this case, the first step involves a barrier of 8.7 kcal mol^{-1} (**TS0**, Figure 7) and leads to **I1 b**′ with an energy release of 18.8 kcal mol^{-1}. Hence, the uncatalyzed aldolization is disfavored from kinetic and thermodynamic viewpoints. The catalyst acts as a Lewis acid by decreasing the LUMO energy (by 0.48 eV) and increasing the LUMO coefficient of the acceptor carbonyl (from 0.691 to 0.993 in the uncomplexed aldehyde and in **R1 b**, respectively), as expected. However, the catalyst also activates the dicarbonyl molecule by proton abstraction and formation of the enolate structure, as suggested by the charges computed by natural population analysis (−0.708 on the donor in **R1 b**). This dual activation leads to a reduced HOMO–LUMO gap upon complexation, from 4.25 to 2.90 eV in the bare enol and in **R1 b**, respectively; thus the electron transfer proceeds more easily during nucleophilic attack.

Likewise, we have estimated the role of the oxide in the following cyclization and dehydration steps. The water-assisted heterocyclization under uncatalyzed conditions proceeds through an earlier transition state (**TS2 bW**′) as the developing N–C bond is longer than that under catalysis (1.668 vs. 1.572 Å) and the Wiberg bond order is lower (0.713 vs. 0.793). In the absence of the MgO surface, an intramolecular H bond (1.960 Å) between the alcohol group and the ester carbonyl stabilizes the transition structure. Notably, the energy barrier for this step in both cases is caused only by entropic effects as the enthalpy barrier is very low (~1 kcal mol^{-1}); however, the entropic effects for the uncatalyzed system are greater than those of the catalyzed clamped structure **TS2 bW**, which leads to a higher free-energy barrier (22.4 for **TS2 bW**′ vs. 9.1 kcal mol^{-1} for **TS2 bW**). The uncatalyzed dehydration of the amino-alcohol moiety takes place through a transition structure (**TS3 bW**′) that involves a moderate barrier (19.0 kcal mol^{-1}), a similar value to that of the catalyzed system but higher in energy (**TS3 bW**′ is 27.7 kcal mol^{-1} higher in energy than **TS3 bW**).

These results suggest that the presence of a framework environment that envelops and supports the reacting species (MgO) not only stabilizes the reacting species but also provides a number of reaction-promoting factors, such as adsorption stability, the reduction of unfavorable entropic effects, the enhancement of collision chances in the correct orientation, and recollision until the accumulating energy rises above the activation barrier.

Finally, an alternative path that involves dehydration in **I1 b** before heterocyclization (Knoevenagel condensation) has been ruled out as the calculations reveal a transition structure, **TS2 bW**″, 15.1 kcal mol^{-1} higher in energy than the reactants, therefore, this is a kinetically less favored route than the path that involves initial heterocyclization and a closing dehydration step.

Conclusion

We report for the first time the Friedländer condensation catalyzed by basic carbon materials, carbon-supported MgO, which lead to the corresponding N-containing heterocyclic compounds of interest. The reaction proceeds under solvent-free and mild conditions. The scope of the methodology has been demonstrated by the reaction of different 2-aminoaryl aldehydes and 1,3-dicarbonyl compounds.

Although a decrease of the surface area and microporosity of the carbon materials under study was observed, our results indicate that MgO is the main catalytically active species responsible of the formation of the corresponding heterocyclic compounds. Remarkably, the activity of the catalysts does not only correlate to the MgO loading but also apparently depends on the available active catalytic surface of the MgO crystals on the hybrid materials.

The carbon support affects the catalytic activity of the investigated materials slightly as demonstrated if the carbon Norit RX3 was used. The lower activity found for Norit RX3 could be because of the changes in the reaction mechanism; π–π stacking interactions between catalyst and substrate could be behind the operative pathway of the reaction.

The computational analysis of the reaction mechanism suggests dual activation by the catalyst, as both carbonyl compounds are activated for the condensation. The catalyst plays a role until the last dehydration step to stabilize the species and promote the reaction. Moreover, the regioselectivity of the condensation for asymmetric dicarbonyl compounds has been justified by the calculations based on energy and electronic factors.

Finally, the advantage of using carbon-supported MgO materials for the Friedländer reaction relies on their easy preparation from a natural MgO source and high thermal stability. These materials constitute a highly efficient, sustainable alternative to amino-grafted and bifunctional mesoporous silicas.

Experimental Section

Catalytic performance

The reactions were followed by TLC chromatography performed on DC-Aulofolien/Kieselgel 60 F_{245} (Merck) using mixtures of CH_2Cl_2/EtOH 98:2 as eluent.

The characterization of the reaction products was performed by ^{1}H NMR spectroscopy. NMR spectra were recorded by using a Bruker AVANCE DPX-300 spectrometer (300 MHz for ^{1}H). ^{1}H chemical shifts (δ) in [D_6]DMSO are referenced to internal tetramethylsilane.

The reactions were performed in the liquid phase under atmospheric pressure by using a multiexperiment work station StarFish (Radley's Discovery Technologies UK).

Typically, 2-aminoaryl aldehyde (0.5 mmol) and the 1,3-dicarbonyl compound (5 mmol) were added to a three-necked vessel of 10 mL capacity, equipped with a condenser, thermometer, and magnetic stirrer (0.8 cm). Subsequently, the catalyst (25 mg) was added and the reaction mixture was stirred (250 rpm) at RT (293 K) for the time indicated in the figures or tables. The samples were withdrawn at different reaction times by diluting a small amount of the reaction mixture in dichloromethane (0.5 mL). Subsequently, the catalyst was collected by filtration, and the solvent evaporated in vacuo.

Theoretical calculations

In a small size range, mass spectra studies have revealed prominent abundances at MgO clusters of tubular structures formed by the stacking of hexagonal $(MgO)_3$ units in addition to the well-known cubic motif.[39] For larger clusters, the appearance of the cubic motif of the MgO bulk can be expected and experimental as well as theoretical evidence for this transition has been found. Many theoretical studies have been performed on neutral and charged MgO clusters using a variety of theoretical approaches.[40] The geometries obtained in these calculations are all in agreement with those suggested by experiments, and a number of tubular isomer geometries were found for $(MgO)_n$ clusters.[41] Hexagonal tubes have been identified by a genetic algorithm[42] as the putative global minima for clusters with $(MgO)_{3k}$ ($k=1$–5). For other cluster compositions, often more cubelike structures are predicted, but there is no common agreement on their structures in the literature yet. A recent combined experimental (gas-phase IR spectroscopy) and theoretical (DFT) investigation gives clear evidence that the $(MgO)_n$ ($n=1$–20) clusters have a hexagonal tube structure,[43] with the exception of $(MgO)_4$.[44] With these precedents in mind, we compared the cubic and hexagonal tubular structures of a $(MgO)_{15}$ cluster. The size $n=15$ was selected as large enough to contain the reactant structures. In agreement with the above conclusions, the hexagonal tube structure was more stable (by 17.3 kcal mol^{-1}). Hence, this structure was chosen for our DFT calculations.

Calculations were performed by using Gaussian09.[45] The B3LYP hybrid DFT method[46] with the 6-31G(d,p) basis set was used to optimize the geometries. B3LYP is a reliable level of theory used commonly in the study of different nanostructures.[47] Vibrational frequencies were also calculated at the same level to confirm that all the stationary points correspond to true minima on the potential energy surface and to extract vibrational zero-point and thermal corrections from the thermodynamic results. Transition state calculations were performed using the same level of theory. The intrinsic reaction coordinate (IRC) pathways[48] have been traced to verify two desired minima connected by the transition states. To obtain insights into the adsorption/desorption processes, relaxed scans of the PES were performed by changing the distance between two key atoms progressively. Electronic parameters, such as frontier molecular orbitals and natural bond orbital (NBO) analyses,[49] and energy calculations, were computed on the optimized structures at the same level.

Acknowledgements

This work has been supported by MICINN (projects CTQ2009–10478 and CTQ2011–27935). We are grateful to the Centro de Supercomputación de Galicia (CESGA) for generous allocation of computing resources.

Keywords: carbon · magnesium · nitrogen heterocycles · reaction mechanisms · supported catalysts

[1] J. Marco-Contelles, E. Pérez-Mayoral, A. Samadi, M. C. Carreiras, E. Soriano, *Chem. Rev.* **2009**, *109*, 2652 – 2671.
[2] a) A. G. Montalban, Heterocycles in Natural Product Synthesis (Eds.: K. C. Majumdar, S. K. Chattopadhyay), Wiley-VCH, Weinheim, **2011** pp. 299 – 339; b) J. Egea, C. de los Rios, *Curr. Top. Med. Chem.* **2011**, *11*, 2807 – 2823; c) S. Madapa, Z. Tusi, S. Batra, *Curr. Org. Chem.* **2008**, *12*, 1116 – 1183.
[3] a) P. Galatsis, K. Yamagata, J. A. Wendt, C. J. Connolly, J. W. Mickelson, J. B. J. Milbank, S. E. Bove, C. S. Knauer, R. M. Brooker, C. E. Augelli-Szafran, R. D. Schwarz, J. J. Kinsora, K. S. Kilgore, *Bioorg. Med. Chem. Lett.* **2007**, *17*, 6525 – 6528.
[4] O. O. Fadeyi, S. T. Adamson, E. L. Myles, C. O. Okoro, *Bioorg. Med. Chem. Lett.* **2008**, *18*, 4172 – 4176.
[5] a) A. Mai, D. Rotili, D. Tarantino, P. Ornaghi, F. Tosi, C. Vicidomini, G. Sbardella, A. Nebbioso, M. Miceli, L. Altucci, P. Filetici, *J. Med. Chem.* **2006**, *49*, 6897 – 6907; b) A. T. Smith, M. R. Livingston, A. Mai, P. Filetici, S. F. Queener, W. J. Sullivan Jr., *Antimicrob. Agents Chemother.* **2007**, *51*, 1109 – 1111.
[6] D. Ramesh, M. T. Chary, E. Laxminarayana, B. Screenivasulu, *Ind. J. Chem. B* **2010**, *49*, 1271 – 1273.
[7] K. Mogilaiah, K. Vidya, *Ind. J. Chem. B* **2007**, *46*, 1721 – 1723.

[8] a) A. Shaabani, E. Soleimani, Z. Badri, *Monatsh. Chem.* **2006**, *137*, 181 – 184; b) M. A. Zolfigol, P. Salehi, M. Shiri, T. F. Rastegar, A. Ghaderi, *J. Iran. Chem. Soc.* **2008**, *5*, 490 – 497; c) B. Das, K. Damodar, N. Chowdhury, R. A. Kumar, *J. Mol. Catal. A* **2007**, *274*, 148 – 152; d) M. Dabiri, S. C. Azimi, A. Bazgir, *Monatsh. Chem.* **2007**, *138*, 659 – 661; e) U. V. Desai, S. D. Mitragotri, T. S. Thopate, D. M. Pore, P. P. Wadgaonkar, *Arkivoc* **2006**, *xv*, 198 – 204; f) M. Narasimhulu, T. S. Reddy, K. C. Mahesh, P. Prabhakar, Ch. B. Rao, Y. Venkateswarlu, *J. Mol. Catal. A* **2007**, *266*, 114 – 117; g) B. Das, M. Krishnaiah, K. Laxminarayana, D. Nandankumar, *Chem. Pharm. Bull.* **2008**, *56*, 1049 – 1051.

[9] D. Garella, A. Barge, D. Upadhyaya, Z. Rodriguez, G. Palmisano, G. Cravotto, *Synth. Commun.* **2009**, *40*, 120 – 128.

[10] S. Chauhan, R. Chakravarti, S. M. J. Zaidi, S. S. Aldeyab, V. Basireddy, A. Vinu, *Synlett* **2010**, *17*, 2597 – 2600.

[11] a) J. López-Sanz, E. Pérez-Mayoral, D. Procházková, R. M. Martín-Aranda, A. J. López-Peinado, *Top. Catal.* **2010**, *53*, 1430 – 1437.

[12] a) F. Domínguez-Fernández, J. López-Sanz, E. Pérez-Mayoral, D. Bek, R. M. Martín-Aranda, A. J. López-Peinado, J. Cejka, *ChemCatChem* **2009**, *1*, 241 – 243; b) J. López-Sanz, E. Pérez-Mayoral, E. Soriano, M. Sturm, R. M. Martín-Aranda, A. J. López-Peinado, J. Cejka, *Catal. Today* **2012**, *187*, 97 – 103; c) A. Smuszkiewicz, J. López-Sanz, E. Pérez-Mayoral, E. Soriano, I. Sobczak, M. Ziolek, R. M. Martín-Aranda, A. J. López-Peinado, *J. Mol. Catal. A* **2013**, *378*, 38 – 46; d) A. Smuszkiewicz, E. Pérez-Mayoral, E. Soriano, I. Sobczak, M. Ziolek, R. M. Martín-Aranda, A. J. López-Peinado, *Catal. Today* **2013**, *218 – 219*, 70 – 75.

[13] a) E. Pérez-Mayoral, J. Cejka, *ChemCatChem* **2011**, *3*, 157 – 159; b) E. Pérez-Mayoral, Z. Musilová, B. Gil, B. Marszalek, M. Položij, P. Nachtigall, J. Čejka, *Dalton Trans.* **2012**, *41*, 4036 – 4044; c) M. Polozij, E. Pérez-Mayoral, J. Cejka, J. Hermann, P. Nachtigall, *Catal. Today* **2013**, *204*, 101 – 107.

[14] J. López-Sanz, E. Pérez-Mayoral, E. Soriano, D. Omenat-Morán, C. J. Durán, R. M. Martín-Aranda, I. Matos, I. Fonseca, *ChemCatChem* **2013**, *5*, 3736 – 3742.

[15] J. Przepiórski, A. Czyżewski, J. Kapica, M. A. de la Casa-Lillo, *Pol. J. Chem. Technol.* **2011**, *13*, 42 – 46.

[16] J. Przepiórski, A. Czyzewski, J. Kapica, D. Moszyński, B. Grzmil, B. Tryba, S. Mozia, A. W. Morawski, *Chem. Eng. J.* **2012**, *191*, 147 – 153.

[17] J. M. Valente Nabais, P. J. M. Carrot, *J. Chem. Educ.* **2006**, *83*, 436 – 438.

[18] A. Nourry, S. Legoupy, F. Huet, *Tetrahedron Lett.* **2007**, *48*, 6014 – 6018.

[19] W. Versées, S. Loverix, A. Vandemeulebroucke, P. Geerlings, J. Steyaert, *J. Mol. Biol.* **2004**, *338*, 1 – 6.

[20] J. L. Kellie, L. Navarro-Whyte, M. T. Carvey, S. D. Wetmore, *J. Phys. Chem. B* **2012**, *116*, 2622 – 2632.

[21] A. Olasz, P. Mignon, F. De Proft, T. Veszprémi, P. Geerlings, *Chem. Phys. Lett.* **2005**, *407*, 504 – 509.

[22] K. Tanabe, M. Misono, Y. Ono, H. Hattori in *Stud. Surf. Sci. Catal. Vol. 51* (Eds.: B. Delmom, J. T. Yates), Kodansha/Elsevier, Tokyo/Amsterdam, **1989**.

[23] T. Ito, T. Tashiro, M. Kawasaki, T. Watanabe, K. Toi, H. Kobayashi, *J. Phys. Chem.* **1991**, *95*, 4476 – 4483.

[24] A. Markovits, J. Ahdjoudj, C. Minot, *Mol. Eng.* **1997**, *7*, 245 – 261.

[25] V. K. Díez, C. R. Apesteguía, J. I. Di Cosimo, *Catal. Today* **2000**, *63*, 53 – 62.

[26] MgO-based catalysts contain basic sites strong enough to abstract the proton from an acetone molecule and are thereby active for the vapor-phase aldol condensation reaction; a) J. I. Di Cosimo, V. K. Diez, C. R. Apestegula, *Appl. Catal. A* **1996**, *137*, 149 – 166; b) G. Zhang, H. Hattori, K. Tanabe, *Appl. Catal.* **1988**, *36*, 189 – 197.

[27] T. F. Dossin, M.-F. Reyners, R. J. Berger, G. B. Marin, *Appl. Catal. B* **2006**, *67*, 136 – 148.

[28] a) C. Di Valentin, A. Del Vitto, G. Pacchioni, S. Abbet, A. S. Wörz, K. Judai, U. Heiz, *J. Phys. Chem. B* **2002**, *106*, 11961 – 11969; b) M. M. Branda, P. G. Belelli, R. M. Ferullo, N. J. Castellani, *Catal. Today* **2003**, *85*, 153 – 165; c) M. M. Branda, A. H. Rodríguez, P. G. Belelli, N. J. Castellani, *Surf. Sci.* **2009**, *603*, 1093 – 1098; d) H. Petitjean, K. Tarasov, F. Delbecq, P. Sautet, J. M. Krafft, P. Bazin, M. C. Paganini, E. Giamello, M. Che, H. Lauron-Pernot, G. Costentin, *J. Phys. Chem. C* **2010**, *114*, 3008 – 3016.

[29] J. L. Anchell, K. Morokuma, A. C. Hess, *J. Chem. Phys.* **1993**, *99*, 6004 – 6013.

[30] a) A. M. Ferrari, S. Huber, H. Knözinger, K. M. Neyman, N. Rösch, *J. Phys. Chem. B* **1998**, *102*, 4548 – 4555; b) K. Todnem, K. J. Børve, M. Nygren, *Surf. Sci.* **1999**, *421*, 296 – 307.

[31] a) J. L. Anchell, A. C. Hess, *J. Phys. Chem.* **1996**, *100*, 18317 – 18321; b) A. L. Almeida, J. B. L. Martins, C. A. Taft, E. Longo, W. A. Lester Jr., *Int. J. Quant. Chem.* **1999**, *71*, 153 – 165; c) B. Ahlswede, T. Homann, K. Jug, *Surf. Sci.* **2000**, *445*, 49 – 59.

[32] J. A. Rodriguez, T. Jirsak, S. Sambasivan, D. Fischer, A. Maiti, *J. Chem. Phys.* **2000**, *112*, 9929 – 9939.

[33] a) J. A. Rodriguez, A. Maiti, *J. Phys. Chem. B* **2000**, *104*, 3630 – 3638; b) Z. Bagheri, M. Moradi, *Struct. Chem.* **2014**, *25*, 495 – 501.

[34] A. Markmann, J. L. Gavartin, A. L. Shluger, *Phys. Chem. Chem. Phys.* **2006**, *8*, 4359 – 4367.

[35] a) R. Soave, G. Pacchioni, *Chem. Phys. Lett.* **2000**, *320*, 345 – 351; b) J. A. Snyder, D. R. Alfonso, J. E. Jaffe, Z. Lin, A. C. Hess, M. Gutowski, *J. Phys. Chem. B* **2000**, *104*, 4717 – 4722.

[36] a) G. Pacchioni, J. M. Ricart, F. Illas, *J. Am. Chem. Soc.* **1994**, *116*, 10152 – 10158; b) S. Livraghi, M. C. Paganini, E. Giamello, *J. Mol. Catal. A* **2010**, *322*, 39 – 44.

[37] A. M. Ferrari, G. Pacchioni, *J. Chem. Phys.* **1997**, *107*, 2066 – 2078.

[38] The loss of water (15.8 kcal mol^{-1}) and the product desorption (19.3 kcal mol^{-1}) lead to the free-energy difference of 35.1 kcal mol^{-1} between **I3 bW** and **I4** shown in Figure 6.

[39] a) W. A. Saunders, *Phys. Rev. B* **1988**, *37*, 6583 – 6586; b) P. J. Ziemann, A. W. Castleman, *J. Chem. Phys.* **1991**, *94*, 718 – 728.

[40] a) M. Recio, R. Pandey, A. Ayuela, A. B. Kunz, *J. Chem. Phys.* **1993**, *98*, 4783 – 4792; b) M. J. Malliavin, C. Coudray, *J. Chem. Phys.* **1997**, *106*, 2323 – 2330; c) E. de la Puente, A. Aguado, A. Ayucla, J. M. Lopez, *Phys. Rev. B* **1997**, *56*, 7607 – 7614.

[41] a) C. Roberts, R. L. Johnston, *Phys. Chem. Chem. Phys.* **2001**, *3*, 5024 – 5034; b) L. Chen, C. Xu, X.-F. Zhang, *THEOCHEM* **2008**, *863*, 55 – 59.

[42] a) R. B. Dong, X. S. Chen, X. F. Wang, W. Lu, *J. Chem. Phys.* **2008**, *129*, 044705 – 044709; b) D. Spagnoli, J. F. Banfield, S. C. Parker, *J. Phys. Chem. C* **2008**, *112*, 14731 – 14736.

[43] a) D. van Heijnsbergen, G. von Helden, G. Meijer, M. A. Duncan, *J. Chem. Phys.* **2002**, *116*, 2400 – 2406; b) M. Chen, A. R. Felmy, D. A. Dixon, *J. Phys. Chem. A* **2014**, *118*, 3136 – 3146.

[44] M. Haertelt, A. Fielicke, G. Meijer, K. Kwapien, M. Sierka, J. Sauer, *Phys. Chem. Chem. Phys.* **2012**, *14*, 2849 – 2856.

[45] Gaussian 09, Revision B.1., M. J. Frisch, G. W. Trucks, H. B. Schlegel, G. E. Scuseria, M. A. Robb, J. R. Cheeseman, G. Scalmani, V. Barone, B. Mennucci, G. A. Petersson, H. Nakatsuji, M. Caricato, X. Li, H. P. Hratchian, A. F. Izmaylov, J. Bloino, G. Zheng, J. L. Sonnenberg, M. Hada, M. Ehara, K. Toyota, R. Fukuda, J. Hasegawa, M. Ishida, T. Nakajima, Y. Honda, O. Kitao, H. Nakai, T. Vreven, J. A. Montgomery, Jr., J. E. Peralta, F. Ogliaro, M. Bearpark, J. J. Heyd, E. Brothers, K. N. Kudin, V. N. Staroverov, R. Kobayashi, J. Normand, K. Raghavachari, A. Rendell, J. C. Burant, S. S. Iyengar, J. Tomasi, M. Cossi, N. Rega, J. M. Millam, M. Klene, J. E. Knox, J. B. Cross, V. Bakken, C. Adamo, J. Jaramillo, R. Gomperts, R. E. Stratmann, O. Yazyev, A. J. Austin, R. Cammi, C. Pomelli, J. W. Ochterski, R. L. Martin, K. Morokuma, V. G. Zakrzewski, G. A. Voth, P. Salvador, J. J. Dannenberg, S. Dapprich, A. D. Daniels, Farkas, J. B. Foresman, J. V. Ortiz, J. Cioslowski, and D. J. Fox, Gaussian, Inc., Wallingford CT, **2009**.

[46] a) A. D. Becke, *J. Chem. Phys.* **1993**, *98*, 5648 – 5652; b) C. Lee, W. Yang, R. G. Parr, *Phys. Rev. B* **1988**, *37*, 785 – 789.

[47] a) M. Moradi, A. A. Peyghan, Z. Bagheri, M. Kamifiroozi, *J Mol Model* **2012**, *18*, 3535 – 3540; b) J. Beheshtian, M. T. Baei, A. A. Peyghan, Z. Bagheri, *J Mol Model* **2012**, *18*, 4745 – 4750.

[48] C. Gonzalez, H. B. Schlegel, *J. Phys. Chem.* **1990**, *94*, 5523 – 5527.

[49] a) A. E. Reed, R. B. Weinstock, F. J. Weinhold, *J. Chem. Phys.* **1985**, *83*, 735 – 746; b) A. E. Reed, L. A. Curtiss, F. J. Weinhold, *Chem. Rev.* **1988**, *88*, 899 – 926.

Received: August 2, 2014
Published online on ■■ ▮▮, 0000

Oxide, outside: MgO supported on carbon is able to catalyze the synthesis of interesting N-containing heterocyclic compounds efficiently under mild conditions. MgO on the carbon surface is responsible for the catalytic behavior. These carbon materials are environmentally friendly catalysts for the Friedländer reaction.

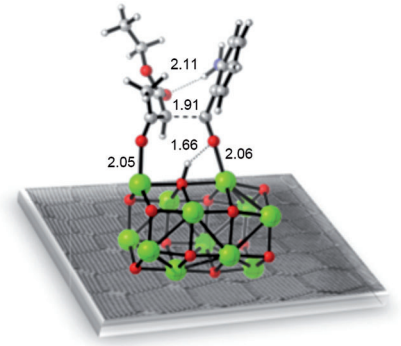

M. Godino-Ojer, A. J. López-Peinado, R. M. Martín-Aranda, J. Przepiórski, E. Pérez-Mayoral, E. Soriano**

■■ – ■■

Eco-Friendly Catalytic Systems Based on Carbon-Supported Magnesium Oxide Materials for the Friedländer Condensation